Spatial behavioural responses to the spread of an infectious disease can suppress Turing and Turing–Hopf patterning of the disease

Alberto d'Onofrio [a,*], Malay Banerjee [b], Piero Manfredi [c]

[a] International Prevention Research Institute, 106 Cours Lafayette, 69006 Lyon, France
[b] Department of Mathematics and Statistics, Indian Institute of Technology Kanpur, Kanpur 208016, India
[c] Department of Economics, Pisa University, Pisa, Italy

A B S T R A C T

Reducing risky behaviour and/or avoiding sites where the risk of infection is perceived as higher (by social and/or spatial distancing) represent the two main forms of non-pharmaceutical behavioural responses of humans to the threats of infectious diseases. Here we investigate, within a reaction–diffusion setting, a family of new models for an endemic SIR (susceptible–infective–removed) infectious disease for which no vaccine is available and individuals' responses to the infection threat are entirely based on changes either in their social behaviour or in their mobility behaviour, that is avoiding to visit sites with a large infection prevalence.

First, we derive general conditions for the onset of Turing patterns for a general family of spatially inhomogeneous SIR models with a prevalence-dependent contact rate and constant recruitment. Then, we characterize our main family of models where the behavioural response also includes a spatial component, and show the condition bringing to the mitigation, or even the destruction, of Turing patterns. The same conditions can allow the transition from Turing–Hopf spatio-temporal patterns to pure Hopf temporal patterns. The same is also done for two SIS models. These results bring an inference of interest: the reduction of spatial clustering typically observed during the course of an epidemics might be related to a combination of agents' spontaneous social and spatial distancing. To validate our theoretical results and further explore other spatio-temporal effects of the proposed spatial behavioural responses, numerical simulations of a specific instance of the above-mentioned family of SIR models have been performed.

1. Introduction

The effects of spatial mobility and spatial diffusion on the spread of infectious diseases have been investigated in many specific models described by different mathematical tools ranging from simple deterministic, spatially implicit, ODE models, to spatially explicit reaction–diffusion PDE models, up to fully stochastic models, ranging from network up to Individual Based Models (IBMs), and a wide body of results is now available [1–6]. Though some recent models are sophisticated and include several structural details on the underlying population (e.g. the IBM models used for pandemic prediction [7–9]) they suffer the shortcoming of most mathematical epidemiology literature, namely the fact they treat

* Corresponding author.
E-mail address: alberto.donofrio@i-pri.org (A. d'Onofrio).

humans as passive actors keeping the same behaviour regardless of the state of the epidemics. This fact, possibly already untrue in the pre-scientific period, is fully denied in the current days by a large body of evidence [10,11]. Important contemporary examples are constituted by the recent Ebola epidemics [12–14] and by 2009 H1N1 flu pandemics [15–17]. However, analysis of Spanish flu data have shown that even one century ago the spread and control of that devastating pandemics were deeply influenced by spontaneous as well as enforced behaviour changes [18–20]. This was shown both for Europe [18,19] and for the USA [20]. This dramatic change of perspective in the relation between humans and infectious diseases has led, during the last 15 years, to the development of the behavioural epidemiology of infectious diseases (BE), a new branch of mathematical epidemiology (see [10,11] and references therein) using a range of multidisciplinary tools to investigate how humans can adapt their behaviour to respond to the threats brought by infections.

However, given that a large part of the behavioural epidemiology research carried out so far has been based on simple models, little work has been done yet to incorporate the agents' behavioural within spatially structured epidemiological models, especially with regard to the area of epidemic models within reaction–diffusion PDE settings. In this area the few attempts to include – mostly indirectly – behavioural components, have followed two main separate directions.

The first one is represented by those efforts including nonlinear cross diffusion terms initiated by [21,22], where susceptible individuals are assumed to be repelled away by the gradient of the function representing the (spatial) prevalence of infective individuals. This area has seen a number of more recent contributions [23–26].

The second direction is represented by those works considering nonlinear incidence rates [27–33], and which extended to reaction–diffusion settings the pioneering paper by Capasso and Serio [34]and later studies [35–37]. The works [27–33] focused on the search for the conditions leading to the onset of Turing bifurcations [2,3,5,38] and of Turing–Hopf instabilities [39]. Turing bifurcations are a hallmark of system complexity that capture a fundamental trait of communicable infectious, namely the tendency of cases to aggregate into spatially clusters [27]. Instead, Turing–Hopf instability [5], characterized by both a temporal and a spatial symmetry breaking, may sometime represent a higher degree of complexity such as spatio-temporal chaos [40]. And chaotic time-series are very frequent in epidemiology of childhood infectious diseases [41]. Very importantly, beside classical models where continuous or regular lattice spaces were considered, many recent epidemiological works have been conducted on network-based structures [11,42–46].

Though the adoption of nonlinear contact rates is indeed a main avenue to incorporate the agents' behavioural responses (see [10,11] and references therein) in no one of previous paper explicit mention of behavioural hypotheses was actually made.

In this work we introduce, within a reaction–diffusion setting, a family of new models for an endemic SIR (susceptible–infective–removed) infectious disease for which no vaccine (or pharmaceutical treatment either) is available and individuals' responses to the infection threat are entirely based on changes in either their social behaviour, or in their mobility behaviour, as in [21,22]. The underlying intuition is that – once awareness of the infection has been acquired – aware individuals respond to the infection by increasing their "'social distancing'" i.e., reducing their contact and transmission rates, and/or by increasing "'spatial distancing'" i.e., avoiding to visit those spatial sites where the local infective prevalence is perceived as relatively larger, as in [21,22]. Arguably, combinations of "'social'" and "'spatial'" distancing have represented the two key forms of humans' behavioural responses to the threats of infectious diseases in mankind history before the advent of pharmaceutical interventions such as vaccination and treatments, as reviewed in [11,47]. Important historical examples are the social and spatial distancing enacted during various plague epidemics, as documented in [48] and in fundamental literary works [49]. For example, the *Decameron* by Giovanni Boccaccio, the *Diary* by Samuel Pepys and various works by William Shakespeare. Moreover, in the absence of pharmaceutical interventions, both forms of distancing remain two main options even in modern societies as documented e.g., by the dramatic decline of travels to Far-East during the SARS crisis – as an example of avoidance of movements towards area perceived as "'high risk'" [50]. Similar large-scale phenomena were also evidenced, although to a lesser extent, during the 2009 H1N1 flu pandemics [51].

In particular our model for behaviour is "'simple'" i.e., we do not include a specific layer for modelling the acquisition of awareness. Therefore, our formulation of social behaviour change is implicit i.e, it is based on a phenomenological relation between the contact (or transmission rate) and the infective prevalence.

Our analysis focuses, from both the biophysics and the public health viewpoints, on a specific problem of epidemiological relevance: the suppression of Turing patterns induced by the spatial behavioural reaction modelled by (2). To achieve this aim, we analyse the proposed family of models in a hierarchical manner. First, we analyse a spatially homogeneous family of SIR models with a general nonlinear contagion rate. Then we re-analyse this family of models by including the spatial structure under the classical hypotheses on diffusion and derive general conditions for Turing instability around the endemic equilibrium. Finally, we include in our family of models also a spatial component in the behavioural response, and provide the conditions ensuring the mitigation, or even the destruction, of Turing patterns. Indeed, a further motivation for the present work based on a general family of models was that all the above cited contributions using nonlinear infection rates [27–33] exhibited – despite their specificity – many similarities, especially in the derivation of the onset of Turing patterns.

The manuscript is organized as follows. Section 2 provides a review of the literature on epidemiological models in reaction diffusion settings including behavioural effects. Section 3 presents and analyses a family of models for an endemic infectious diseases with spontaneous agents' behaviour responses in the absence of spatial structure. The analysis of the basic spatial version of the model is reported in section four. In section five the full model also including spatial distancing is reported. Sections six and seven extend the analysis to the case of an SIS (susceptible–infective–susceptible) infection. In Section 8 we propose and numerically investigate a specific SIR behavioural model belonging to the above-mentioned family in order to verify and fine-tune our theoretical results and obtain further results. Concluding remarks follow.

2. Spatial epidemiological models with behavioural responses: a review of the literature

Milner and coworkers introduced [21,22] a modification of the spatial version of Kermack and McKendrick SIR model [1] where they added to the "'classical'" term repelling individuals (irrespective of their epidemiological state) away from crowded areas, a truly behavioural term repelling susceptible individuals from sites characterized by large prevalence of infective individuals. Consequently they modelled the spatial flux of susceptible individuals including the gradient of infectives [21,22]

$$J_S = -aS\nabla N - cS\nabla I \tag{1}$$

where $S(x,t)$ denotes the density of susceptible subjects, $N(x,t)$ the population density, $a > 0$ and $c > 0$.

Here we assume that only the second phenomenon is enacted as a spatial component of the behavioural response of healthy subjects to which one has to add the diffusive flow of the susceptible:

$$J_S = -D_S\nabla S - cS\nabla I, \tag{2}$$

where $I(x,t)$ is the density of infectious subjects.

Given a compartmental population model u fluxes of the type

$$J_i = -\sum_{j=1}^{n} D_{i,j}^{(0)}\nabla u_j - u_i\sum_{j\neq i} D_{i,j}\nabla u_j, \tag{3}$$

where $D_{i,j} > 0$ and $D_{i,j}^{(0)} > 0$, first introduced in mathematical epidemiology by Capasso and coworkers [52] are termed in the literature non linear cross-diffusion fluxes.

At the best of our knowledge the current mathematical epidemiology literature has only focused on problems of existence, uniqueness and positiveness of the solution of the resulting dynamical systems. For example, in [23] Bendhamane and Langlais provided, under some parametric constraints, existence results for nonnegative solutions of a SIR epidemic model characterized by nonlinear cross–diffusion for all the three epidemic classes and by absence of births (but presence of death). However, no justification was given for the presence of nonlinear cross diffusion.

As far as the non-negativity of solutions of models where our behavioural assumption (2) is concerned, we provide in the appendix a mesoscopic derivation showing that $S(x,t)$ cannot become negative. Our aim is to focus on the physics of the phenomenon, thus we will use informal mathematical derivation.

The following nonlinear cross diffusion flux in the susceptible:

$$J_S = -a(S,I)\nabla S - c(S,I)\nabla I$$

(2) was introduced first by Berres and Ruiz–Baier in [24] (see also [25,26]), who also gave an implicit behavioural description of the flux, in the context of a specific SI model. They investigated two specific cases: $c(S,I) = c_0 > 0$ (i.e. classical linear cross-diffusion) and $c(S,I) = c_0 SI(c_1 - S - I)_+$ with $c_1 > 0$. The focus of their investigation was on defining new numerical methods and, from the modelling viewpoint, on the cross-diffusion driven onset of spatial patterns.

Finally, recent research in ecology and eco-epidemiology has proposed models where an animal behaviour effect was included to mirror a population (for example of predators or of male animals) following another population (for example of preys or female animals) over space [53–55]. This would correspond, in the simple framework of our model to the case of $c < 0$. By adopting (with abuse of meaning) a terminology of theoretical cellular biology [56] our model describe a chemorepulsion-like phenomenon, whereas models [53–55] are chemotaxis-like model. Two opposite phenomena. Moreover, in our model the chemorepulsion-like behaviour is aimed at reducing the contagion of the disease, whereas in [53–55] the chemotaxis-like behaviour is caused by disease-unrelated bio-phenomena.

In the forthcoming sections we propose a general family of models combining nonlinear cross diffusion – mimicking a behaviour – related reduced mobility of at risk individuals, with an appropriate functional specification of the infection incidence, mimicking social-distancing — to represent the overall behavioural response to the infection threat in a situation where no vaccination or treatments are available.

3. A general family of SIR models for behaviour change: the space-homogeneous case

Our general formulation considers an SIR-type infection which is endemic in a stationary population and for which neither prevention through vaccination nor pharmaceutical control measures are available. To make our presentation as smooth as possible we depart from the space-homogeneous case in the absence of any behavioural responses.

3.1. General SIR models for behaviour change: the space-homogeneous case without behavioural response

Let S_*, I_*, R_* denoted the numbers of individuals who at time t are susceptible, infectious, and recovered respectively. Our formulation reads as follows:

$$\frac{d}{dt}S_* = \zeta - \mu S_* - C_*(S_*, I_*) \tag{4}$$

$$\frac{d}{dt}I_* = C_*(S_*, I_*) - (\nu + \mu)I_* \tag{5}$$

$$\frac{d}{dt}R_* = \nu I_* - \mu R_* \tag{6}$$

where $\nu > 0$ is the (constant) recovery rate, $\mu > 0$ is the (constant) mortality rate, $\zeta > 0$ the (constant) recruitment rate, and finally $C_*(S_*, I_*) > 0$ is the overall infection rate, also termed the infection incidence rate.

The overall population $N = S + I + R$ obeys

$$\frac{d}{dt}N = \zeta - \mu N$$

In what follows we assume that the population has achieved its steady state

$$N_{ss} = \frac{\zeta}{\mu}$$

and normalize the state variables and the infection rate as follows

$$(S, I, R) = \frac{1}{N_{ss}}(S_*, I_*, R_*)$$

$$C(S, I) = \frac{1}{N_{ss}}(N_{ss}S, N_{ss}I).$$

Given that $R = 1 - S_{ss} - I_{ss}$ we can disregard the R variable obtaining the system:

$$\frac{d}{dt}S = \mu(1 - S) - C(S, I) \tag{7}$$

$$\frac{d}{dt}I = C(S, I) - (\nu + \mu)I \tag{8}$$

As regards the (normalized) infection rate $C(S, I)$, we assume it is a continuous function with the following properties: (i) no flux from the susceptible to the infectious compartments exists in absence of infectious subjects (no epidemics) or of susceptible (theoretical removal by quarantine or vaccination of all the healthy population)

$$C(S, 0) = C(0, S) = 0;$$

(ii) the larger is the infectious prevalence the larger is the infection rate

$$\partial_I C(S, I) > 0;$$

(iii) the larger is S the larger is the infection rate

$$\partial_S C(S, I) > 0.$$

3.2. General SIR models for behaviour change: the space-homogeneous case with behaviour response

To include the behavioural component we next suppose that the population is able to enact measures to reduce the risk to acquire the infection. In the practise, individuals can achieve this by reducing their social contact rate (i.e., the average number of social contacts per unit of time) and/or by reducing the transmission probability per single social contact. In our general formulation, which does not specify these parameters in an explicit manner, the risk reduction will be represented by a suitable continuous and decreasing function of prevalence $\phi(I)$ multiplying the incidence rate. The transmission model has to be modified as follows:

$$\frac{d}{dt}S = \mu(1 - S) - \phi(I)C(S, I) \tag{9}$$

$$\frac{d}{dt}I = \phi(I)C(S, I) - (\nu + \mu)I \tag{10}$$

where the function $\phi(I)$, $0 \leq \phi(I) \leq 1$ is such that: (i) no risk reduction is observed at very low prevalence levels:

$$\phi(0) = 1$$

(ii) the function is decreasing:

$$\phi'(I) < 0.$$

Henceforward we will call the incidence rate in absence of behavioural response, $C(S, I)$, the baseline, or *normal* incidence rate (NIR), while we will call the incidence rate

$$\Psi(S, I) = \phi(I)C(S, I)$$

the behavioural incidence rate (BIR).

Note that the introduction of the behavioural response affects the infection transmission because the sign of $\partial_I \Psi$ is no more determined a priori. This happens in situations where I is sufficiently large so that the decrease of ϕ is able to compensate the increase of C thus giving $\partial_I \Psi < 0$.

Model (9)–(10) always admits a disease free equilibrium $DFE = (1, 0)$. Setting

$$(S, I) = (1 - u, v)$$

with $0 < u \ll 1$ and $0 < v \ll 1$ and writing

$$\Psi(1 - u, v) \approx a v^p$$

the equation for I at the DFE reads:

$$v' = a v^p - (\mu + \nu) v,$$

implying that for $p < 1$ then the DFE is unstable, for $p > 1$ then the DFE is always stable. Note that for $p = 1$ the condition for the LAS of the DFE is

$$\frac{a}{\mu + \nu} < 1.$$

which allows to give the parameter $a/(\mu + \nu)$ the interpretation of basic reproduction number (BRN) of the infection considered. From the differential inequality:

$$\frac{dI}{dt} = \Psi(S, I) - (\nu + \mu) I \leq \Psi(1 - I, I) - (\nu + \mu) I,$$

it follows that if for $I > 0$

$$\Psi(1 - I, I) < (\nu + \mu) I$$

then the DFE is Globally stable.

As regards the existence of endemic equilibria $EE = (S_e, I_e) > (0, 0)$, from $(S + I)' = 0$ it follows that

$$S = 1 - (1 + \rho) I,$$

where $\rho = (\nu/\mu) \gg 1$. As a consequence, $I' = 0$ implies that:

$$\Psi(1 - (1 + \rho) I, I) = (\nu + \mu) I \tag{11}$$

Eq. (11) is generic, and it can have none, one or more than one (typically two) positive solutions. In other words, the system can have none, one or multiple endemic equilibria.

The Jacobian matrix J at an endemic equilibrium is such that

$$J_{11} = -\mu - \partial_S \Psi(S_e, I_e), J_{12} = -\partial_I \Psi(S_e, I_e), J_{21} = \partial_S \Psi(S_e, I_e), J_{22} = \partial_I \Psi(S_e, I_e) - (\mu + \nu)$$

Remark. In the following, for the sake of notational simplicity we will write $\partial_S \Psi$ and $\partial_S \Psi$ instead of, respectively, $\partial_S \Psi(S_e, I_e)$ and $\partial_I \Psi(S_e, I_e)$.

From the characteristic polynomial

$$\lambda^2 - (J_{11} + J_{22})\lambda + J_{11} J_{22} - J_{12} J_{21}$$

the standard conditions for the local stability are: (i) $-(J_{11} + J_{22}) > 0$, i.e.

$$2\mu + \nu + \partial_S \Psi - \partial_I \Psi > 0 \tag{12}$$

and $J_{11} J_{22} - J_{12} J_{21} > 0$, i.e.

$$\mu(\mu + \nu - \partial_I \Psi) + (\mu + \nu) \partial_S \Psi > 0 \tag{13}$$

If at an endemic equilibrium point EE the previous conditions are not fulfilled, then the EE is unstable.

The global behaviour of the system can be quite complex, and needs to consider specific examples of $\Psi(S, I)$. In other words we ought to renounce to work at level of the entire family of models to move to the study of specific subcases. There is nonetheless one important case where the analysis remains fully general which is the case where the EE is unique and the DFE is unstable. In this case Yakubovich theorem [57] implies that the solutions of the system will be oscillating (either periodically or aperiodically: the type of oscillations depends on the specific model and it cannot be predicted analytically).

Since we want both to keep our analysis at level of meta-models and to focus on spatial patterning, in this work we will not proceed further in the investigation of specific subcases.

4. The spatially structured case with behaviour change and turing patterns

In this section we will consider the baseline spatial version of the model of the previous section where the agents' behavioural responses do not involve their mobility patterns i.e., individuals keep the same mobility regardless of their epidemiological status. The model then reads as follows:

$$\partial_t S = D_S \Delta S + \mu(1 - S) - \Psi(S, I) \tag{14}$$

$$\partial_t I = D_I \Delta I + \Psi(S, I) - (\nu + \mu) I \tag{15}$$

$$\partial_n I|_{\partial\Omega} = \partial_n S|_{\partial\Omega} = 0 \tag{16}$$

Many complex phenomena can of course arise, but here we are mainly interested to the onset of Turing patterning around *a spatially homogeneous locally stable endemic equilibrium EE*. By linearizing spatio-temporally around the endemic equilibrium, and applying the Fourier's transform one gets the following spatio–temporal Jacobian matrix [3]

$$J_{ST}(k) = J(EE) + Diag(-D_S k^2, -D_I k^2)$$

whose characteristic polynomial reads

$$\lambda^2 + a_1(k)\lambda + a_0(k) = 0$$

where

$$a_1(k) = (D_S + D_I)k^2 - (J_{11} + J_{22}) > 0$$

$$a_0(k) = D_S D_I k^4 - (D_I J_{11} + D_S J_{22})k^2 + (J_{11} J_{22} - J_{12} J_{21})$$

Thus, since (due to the postulated local stability of the endemic equilibrium) it holds $a_1(k) > 0$ and $a_0(0) > 0$, then the condition to have spatial frequencies that can destabilize *EE* is constituted by the following two inequalities [3,27]

$$D_I J_{11} + D_S J_{22} > 0 \tag{17}$$

$$(D_I J_{11} + D_S J_{22})^2 > 4 D_S D_I (J_{11} J_{22} - J_{12} J_{21}) \tag{18}$$

It is easy to show that conditions (17)–(18) can be summarized into the following constraint:

$$D_I J_{11} + D_S J_{22} > 2\sqrt{D_S D_I a_0(0)} \tag{19}$$

Since the r.h.s. of (19) automatically implies the LAS condition (13), otherwise one would have an imaginary number, it follows that (19) must only be complemented by (12).

Despite the fact we are considering a family of models, the above conditions provide interpretable and useful information. For example by rewriting (19) as follows:

$$D_S\,(\partial_I \Psi - (\mu + \nu)) > D_I(\mu + \partial_S \Psi) + 2\sqrt{D_S D_I a_0(0)} \tag{20}$$

we obtain two results: (i) if $\partial_I \Psi \leq (\mu + \nu)$ then no Turing patterns can occur; (ii) since from (12) ($J_{22} < -J_{11}$), it holds that

$$\partial_I \Psi - (\mu + \nu) < \mu + \partial_S \Psi \Rightarrow \partial_I \Psi - (\mu + \nu) = (\mu + \partial_S \Psi)(1 - F^2)$$

then one can rewrite (20) in the following form:

$$D_S > \frac{D_I}{1 - F^2} + \alpha_0^2 \tag{21}$$

i.e. the Turing pattern can only occur for diffusion coefficients of susceptible individuals that are larger than the diffusion coefficients of the Infectious, which is what we obviously expect in normal conditions.

By resorting to specific subcases of function $\Psi(S, I)$ one can study the ensuing specific type of patterns by the method of the amplitude equation [3,58].

5. Spatial distancing and its impact on spatial patterning

Model (14)–(15), although including the individuals' behavioural response - i.e., what we nowadays term "'social-distancing"' - in the presence of spatial movements, is incomplete as it lacks a spatial component in the behavioural response, what we previously termed "'spatial distancing"'. We therefore now amend model (14)–(15) by adding to the *spatial* flow ψ of susceptible subjects a component that goes in direction opposite to the gradient of the spatial density of infectious individuals. This yields:

$$\psi = -D\nabla S - \bar{A} S \nabla I,$$

where $\bar{A} > 0$. This modelling of spatial behavioural response is remindful of the phenomenon of chemorepulsion, which is the opposite of chemotaxis. The resulting model reads:

$$\partial_t S = D_S \Delta S + div(\bar{A} S \nabla I) + \mu(1 - S) - \Psi(S, I) \tag{22}$$

$$\partial_t I = D_I \Delta I + \Psi(S, I) - (\nu + \mu) I \tag{23}$$

$$\partial_n I|_{\partial\Omega} = \partial_n S|_{\partial\Omega} = 0 \tag{24}$$

After linearizing around a space-homogeneous stable but spatially-patterned endemic state, and applying the Fourier transform, we obtain the following spatio-temporal jacobian matrix:

$$J^*_{ST} = \begin{bmatrix} J_{11} - D_S k^2 & J_{12} - Ak^2 \\ J_{21} & J_{22} - D_I k^2 \end{bmatrix} \tag{25}$$

where $A = \bar{A} S_{EE}$. The characteristic polynomial associated to J^*_{ST} is

$$\lambda^2 + b_1(k)\lambda + b_0(k) = 0$$

where $b_1(k) = a_1(k)$ and $b_0(k) = a_0(k) + J_{21} A k^2$ yielding:

$$b_0(k) = D_S D_I k^4 + (J_{21} A - (D_I J_{11} + D_S J_{22}))\, k^2 + (J_{11} J_{22} - J_{12} J_{21}) \tag{26}$$

Since $J_{21} > 0$ it immediately follows that if

$$A > A_{cr} := \frac{D_I J_{11} + D_S J_{22} - 2\sqrt{D_S D_I b_0(0)}}{J_{21}} \tag{27}$$

then the homogeneous endemic equilibrium is LAS.

The previous result is very clear. In words, if the behavioural spatial response, summarized by coefficient A is sufficiently large, then the Turing pattern disappears.

For $A < A_{cr}$ in the Fourier space there exists an interval of frequencies $(k_1(A), k_2(A))$ such that the system is unstable. Setting

$$h_0 = \frac{b_0(0)}{D_S D_I}, h_1 = \frac{D_I J_{11} + D_S J_{22}}{D_S D_I}, B = \frac{J_{21} A}{D_S D_I}$$

we have

$$k_1^2(B) = \frac{h_1 - B}{2} - \frac{1}{2}\sqrt{(B - h_1)^2 - 4h_0} \tag{28}$$

thus

$$\partial_B k_1^2(B) = -\frac{1}{2} - \frac{1}{2}\frac{(B - h_1)}{\sqrt{(b - h_1)^2 - 4h_0}} = \frac{1}{2}\frac{1}{\sqrt{(B - h_1)^2 - 4h_0}}\left((h_1 - B) - \sqrt{(b - h_1)^2 - 4h_0}\right) > 0 \tag{29}$$

and

$$k_2^2(B) = \frac{h_1 - B}{2} + \frac{1}{2}\sqrt{(B - h_1)^2 - 4h_0} \tag{30}$$

thus

$$\partial_B k_2^2(B) = -\frac{1}{2} + \frac{1}{2}\frac{(B - h_1)}{\sqrt{(b - h_1)^2 - 4h_0}} = \frac{1}{2}\frac{1}{\sqrt{(B - h_1)^2 - 4h_0}}\left((-h_1 + B) - \sqrt{(b - h_1)^2 - 4h_0}\right) < 0 \tag{31}$$

In other words, as it was expected, if the bifurcation parameter A approaches A_{cr} then the size of the instability interval reduces. This means that if A increases but remains lower than A_{cr} then the range of spatial frequencies composing the Turing pattern reduces. At A lower but close to A_{cr}, let us say at $A = A_{cr}(1-\varepsilon)$ with $0 < \varepsilon \ll 1$, the pattern is approximately formed in 1D by a single frequency, in 2D by a circle of frequencies etc... As a consequence varying $A \in (0, A_{cr})$ induces a pattern transitions.

6. Spatial distancing annihilation of Hopf–Turing instabilities

In the previous sections we assumed that the spatially uniform endemic equilibrium was LAS. Thus it was $a_1(k) > 0$ and we had, in absence of spatial distancing, only two scenarios: (Sc1) $a_0(k) > 0$ for all k, meaning that the spatially uniform endemic equilibrium remained LAS; (Sc2) $a_0(k) < 0$ for some k, i.e. onset of Turing instability.

Suppose now that the spatially uniform model is such that, depending on some parameter ζ, instability of the endemic state arises through a Hopf bifurcation at $\zeta = \zeta_{Hopf}$. At least for sufficiently close values of ζ_{Hopf} the determinant of J remains positive so that we can write:

$$\lambda^2 - 2z\omega_0\lambda + \omega_0^2$$

where $\omega_0 > 0$ is the damped oscillation pulsation and $z \in (0, 1)$ is the damping coefficient. It follows that

$$a_1(k) = (D_S + D_I)k^2 - 2z\omega_0.$$

This yields two additional scenarios. The first one (Sc3) is characterized by the fact that, although a $a_0(k) > 0$ for all k it is $a_1(k) < 0$ for

$$0 \leq k^2 < k_H^2 = \frac{2z\omega_0}{D_S + D_I}$$

The resulting Instability is termed spatio-temporal Hopf instability. Often it is said that (Sc3) is characterized by oscillations in time and uniformity in space, however this only approximately holds if $k_H \ll 1$. In the second additional scenario (Sc4), it occurs a $a_1(k) < 0$ for some k but also $a_0(k)$ can be negative for some k. The scenario (Sc4) is termed Hopf–Turing instability and it is characterized by the breaking of both the temporal and the spatial symmetry.

As we have seen the impact of the social distancing in the characteristic polynomial is null w.r.t. the first order degree: $b_1(k) = a_1(k)$ but it is important on the zero degree term: $b_0(k; A) = a_0(k) + J_{12}Ak^2$. Thus social distancing cannot eliminate scenario (Sc3). On the contrary the social distancing term can destroy the Turing–Hopf instability – i.e. (Sc4)– by making $b_0(k; A) > 0$ provided that $A > A_{cr}$, i.e. that (27) holds.

7. SIS model with constant recruitment

Here we briefly investigate the case of the SIS model with constant recruitment of susceptible subjects and spatial behavioural response, which reads as follows:

$$\partial_t S = \theta I + D_S \Delta S + div(\bar{A} S \nabla I) + \mu(1 - S) - \Psi(S, I) \tag{32}$$

$$\partial_t I = D_I \Delta I + \Psi(S, I) - (\mu + \theta)I \tag{33}$$

$$\partial_n I|_{\partial\Omega} = \partial_n S|_{\partial\Omega} = 0 \tag{34}$$

Proceeding as in the previous section, we get the following characteristic polynomial for the spatio–temporal Jacobian matrix:

$$\lambda^2 + a_1(k)\lambda + a_0(k) \tag{35}$$

where:

$$a_1(k) = (D_S + D_I)k^2 + 2\mu + \theta + \partial_S\Psi - \partial_I\Psi$$

$$a_0(k) = b_2k^4 + b_1k^2 + b_0 = D_SD_Ik^4 + (\partial_S\Psi A + (\mu + \partial_S\Psi)D_I + (\mu + \theta - \partial_I\Psi)D_S)\, k^2 + \mu(\mu + \theta + \partial_S\Psi - \partial_I\Psi)$$

As a consequence, the conditions to have a Turing pattern are:

$$2\mu + \theta + \partial_S\Psi - \partial_I\Psi > 0 \tag{36}$$

$$\mu + \theta + \partial_S\Psi - \partial_I\Psi > 0 \tag{37}$$

$$(\mu + \partial_S\Psi)D_I + (\mu + \theta - \partial_I\Psi)D_S + \partial_S\Psi A < -2\sqrt{D_SD_Ib_0} \tag{38}$$

However, note that condition (37) implies condition (36), implying that: **(i)** in absence or presence of behavioural response there cannot be a Hopf (or a Hopf–Turing) bifurcation; **(ii)** the condition for Turing pattern existence in absence of behavioural response is given by (37) and

$$(\mu + \partial_S\Psi)D_I + (\mu + \theta - \partial_I\Psi)D_S < -2\sqrt{D_SD_Ib_0}. \tag{39}$$

Condition (39) can be rewritten as follows:

$$(\mu + \partial_S\Psi)(D_I - D_S) + (\partial_S\Psi + 2\mu + \theta - \partial_I\Psi)D_S < -2\sqrt{D_SD_Ib_0},$$

which implies that if $D_I \geq D_S$ then condition (39) is never fulfilled; **(iii)** the condition of pattern presence if $A > 0$ is given by (37) and (38); **(iv)** The condition for the suppression of the Turing pattern is given by (37) and (39) and

$$A > A_{cr} = \frac{-(\mu + \partial_S\Psi)D_I + (-\mu - \theta + \partial_I\Psi)D_S - 2\sqrt{D_SD_Ib_0}}{\partial_S\Psi} \tag{40}$$

8. A SIS model with vital dynamics

In the previous sections we considered models with constant recruitment of susceptible. Here we briefly consider the case of a SIS model with equal birth and death rates and no recruitment:

$$\partial_t S = D_S \Delta S + div(\bar{A} S \nabla I) + \mu I - \Psi(S, I) + \theta I \tag{41}$$

$$\partial_t I = D_I \Delta I + \Psi(S, I) - (\mu + \theta) I \tag{42}$$

$$\partial_n I|_{\partial\Omega} = \partial_n S|_{\partial\Omega} = 0 \tag{43}$$

The non-spatial version of the model has the following conserved quantity:

$$S + I = S(0) + I(0) = N(0),$$

which is the population size, which we again assume normalized at one, yielding:

$$I' = \Psi(1 - I, I) - (\mu + \theta) I \tag{44}$$

So the endemic equilibrium points I_e of (44) are of the type

$$EE_{**} = (1 - I_e, I_e).$$

At the endemic equilibrium point of (44) the linearized equation reads as follows:

$$i' = -i(\mu + \theta + \partial_S \Psi - \partial_I \Psi)$$

So that the local stability condition in absence of spatial diffusion reads:

$$\mu + \theta + \partial_S \Psi - \partial_I \Psi > 0 \tag{45}$$

The spatio-temporal Jacobian matrix at EE_{**} has a characteristic polynomial such that

$$a_1(k) = (D_S + D_I) k^2 + \mu + \theta + \partial_S \Psi - \partial_I \Psi$$

$$a_0(k) = D_s D_I k^4 + (\partial_S \Psi (A + D_I) + D_S(\mu + \theta - \partial_I \Psi))\, k^2$$

Consequently, the condition to have Turing instability reads as follows:

$$\partial_S \Psi (A + D_I) + D_S(\mu + \theta - \partial_I \Psi) < 0$$

which (taking into account the condition (45) is convenient to rewrite as follows:

$$\partial_S \Psi (A + D_I - D_S) + D_S(\partial_S \Psi + \mu + \theta - \partial_I \Psi) < 0 \tag{46}$$

It follows that: (i) if $A = 0$ then to have Turing instability it must hold (45) and (D_S, D_I) must be so that

$$\partial_S \Psi (D_I - D_S) + D_S(\partial_S \Psi + \mu + \theta - \partial_I \Psi) < 0, \tag{47}$$

implying that also for this family of models Turing instability never occur if $D_I \geq D_S$; (ii) in presence of behavioural spatial response ($A > 0$) to have a Turing instability it must hold (45) and (46); (iii) to destroy the Turing instability observed in absence of A it must hold (45) and

$$\partial_S \Psi (A + D_I) + D_S(\mu + \theta - \partial_I \Psi) > 0 \tag{48}$$

9. Numerical simulations

In this section we numerically we investigate and extend a specific SIR model to corroborate and further expand our theoretical results.

9.1. The Sun model: pattern analysis in absence and presence of spatial behavioural response

For the sake of the comparison, we start considering the SIR model proposed by Sun in [31] and further investigated in [27], which is a spatio-temporal version of a specific sub-case of the well-known family of models proposed by Liu, Hetcothe and Levin in 1987 [59]. The Sun model, which is in turn a particular instance of the family of models (9)–(10), does not depend on human behaviour, so that $\phi(I) = 1$. The contagion rate reads as follows: $C(S, I) = \beta S I^2$, and $\psi(S, I) = C(S, I) = \beta S I^2$, which yields:

$$\partial_t S = D_S \Delta S + \mu(1 - S) - \beta I^2 S \tag{49}$$

$$\partial_t I = D_I \Delta I + \beta I^2 S - (\mu + \nu) I \tag{50}$$

with Neumann boundary conditions.

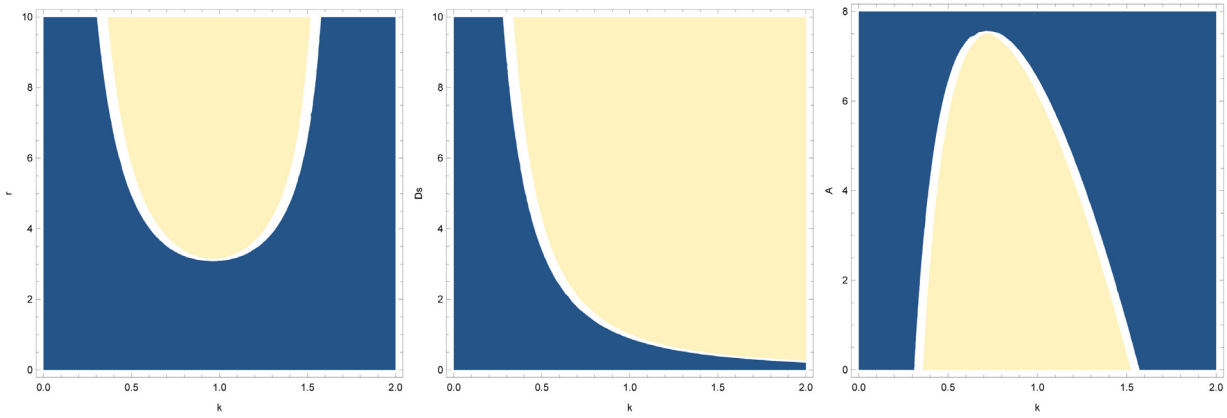

Fig. 1. Model (49)–(50) and its behavioural extension (51)–(50). Impact of (D_S, D_I) on Turing Instability vs Local Stability for $A = 0$ (left and central panels) and $A > 0$ (right panel). Local Stability regions are dark, Turing instability regions in light colours. Right Panel: Stability Region with respect to the parameter $r = D_S/D_I$ and to the spatial frequency $|k|$; Central Panel Stability Region with respect to the parameter D_S and to the spatial frequency $|k|$; Right Panel: Stability Region (for $D_S/D_I = 10$) with respect to the parameter A and to the spatial frequency $|k|$.

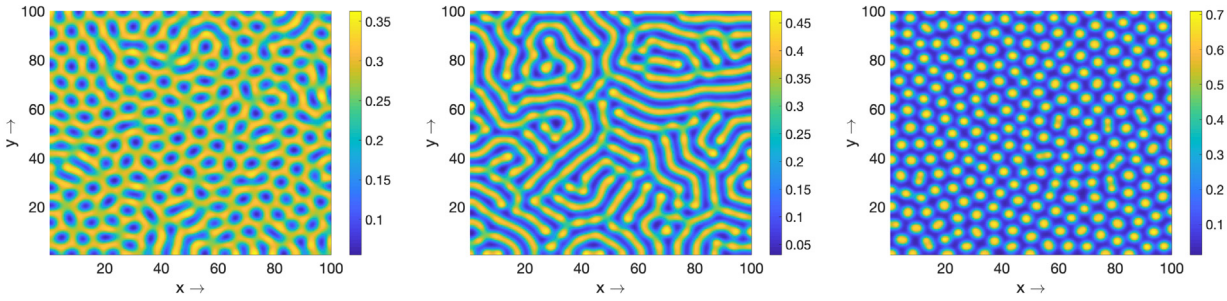

Fig. 2. Model (49)–(50): Turing patterns dependence on D_S for $D_I = 1$. Left panel : $D_S = 3.5$; Central panel: $D_S = 5$; Right panel: $D_S = 10$; Other parameters: see the text.

We start with the baseline case of absence of spatial behavioural reaction, i.e. $\bar{A} = 0$. In [27,31] the author performs a complete bifurcation analysis assuming as key parameters the transmission rate β and the recovery rate ν for fixed values of the diffusion coefficients: $D_S = 6$, $D_I = 1$.

Here, instead we go further than the analysis of [27,31]. Namely, by setting $\beta = 35$, $\mu = 1$ and $\nu = 1.8$ (as in the main case of [31]) we performed a bifurcation analysis where the bifurcation parameters are the two diffusion coefficients D_S and D_I. We obtained that the Turing bifurcation occur provided that the ratio $r = D_S/D_I$ is $r > 3.11$ about, as shown in left panel of Fig. 1.

Moreover, in the limit case $D_I = 0$ a Turing-like bifurcation always occurs, since it exists a $\bar{k}(D_S)$ such that for $k > \bar{k}$ the endemic equilibrium is unstable (see right panel of Fig. 1).

As in [31], we considered $\Omega = [0, 200] \times [0, 200]$ however, we used a smaller spatial step of $\Delta x = \Delta y = 0.5$ and a much smaller timestep $\Delta t = 0.001$ than the ones used in [31]. We adopted as initial condition the following perturbation of the endemic equilibrium

$$(S(0, x, y), I(0, x, y)) = (S_{EE}(1 + \rho_S(x, y)), I_{EE}(1 + \rho_I(x, y)),)$$

where $\rho_S(x, y)$ and $\rho_I(x, y)$ are two piecewise constant bounded stochastic processes, which in each square of the discretization mesh assume a random value uniformly distributed in $(-0.01, 0.01)$. We used as IC the same single instance of the above-described stochastic process for all simulations. In our simulations we set $D_I = 1$ and, as final time, we generally used values t_f such that $t_f \gg 1/(\mu + \nu)$.

The simulation of the model (49)–(50), i.e. at $A = 0$, for $D_I = 1$ is shown in Fig. 2 for three different values of D_S. With the increase in magnitude of D_S we can see that the resulting pattern changes from cold spot to hot spot pattern through labyrinthine pattern. The population density within a patch increases significantly if we compare the range of colour bars in Fig. 2(c) with that of Fig. 2(d).

A consolidated pattern diagram for susceptible and infected population for a range of values of D_S and D_I is presented in Fig. 3.

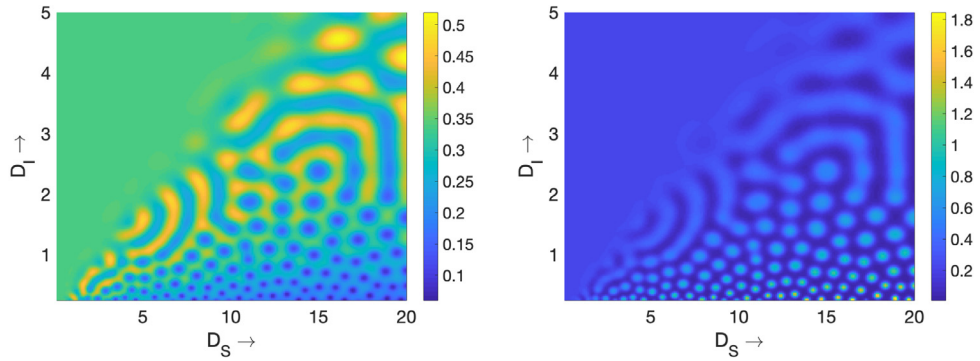

Fig. 3. Model (49)–(50). Visual Summary of Spatial Turing patterns exhibited by S (panel(a)) and I (panel(b)) for a range of values of D_S and D_I.

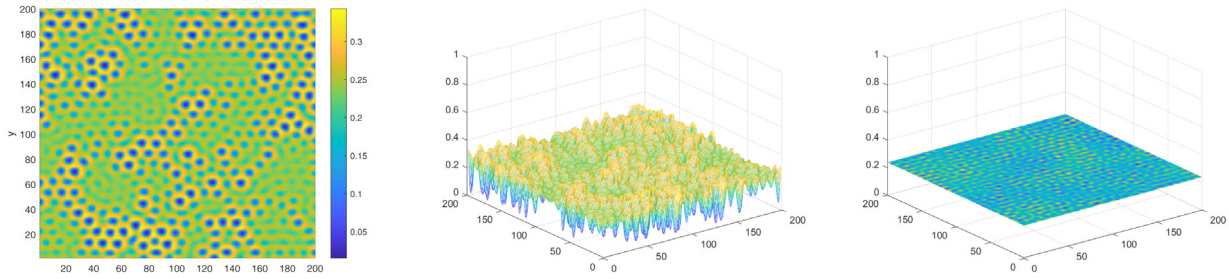

Fig. 4. Model (51)–(50). Spatial impact of social–distancing parameter A on the steady state I. Left and central panel: density and mesh plots of $I(t_f, x, y)$ for $A \approx 0.97A_{cr}$. Right panel: mesh plot of $I(t_f, x, y)$ for $A \approx 1.03A_{cr}$. Initial conditions and other parameters as specified in the text.

Then we modified the model by adding the social-distancing term $div(\bar{A}S\nabla I)$, yielding the following modified PDE for S:

$$\partial_t S = D_S \Delta S + \mu(1 - S) + div\left(\bar{A}S\nabla I\right) - \beta I^2 S \tag{51}$$

The stability region for $r = 10$ is shown in right panel of Fig. 1. With the above specified parametrization, the threshold value for the Turing bifurcation is $A_{cr} \approx 7.54$ for $r = 10$.

The left and central panels of Fig. 4 shows that for $A \approx 0.97A_{cr}$ the endemic equilibrium is unstable, whereas, as shown in the right panel of Fig. 4, for $A \approx 1.03A_{cr}$ the local stability is recovered, and $I(t_f, x, y) \approx I_{EE}$. Note that for values of A close to A_{cr} we expected (and observed) a critical slowing down, so that a large final time was set. For example, for $A = 1.02A_{cr}$ we set $t_f = 2000$.

The behaviour of the system for $0 < A < A_{cr}$ is of interest. We mentioned that we observed a spotted steady state pattern for I at both $A = 0$ (right panel of Fig. 2) and $A = 0.97$ (left panel of Fig. 4). One could think, thus, that the effect of A was simply of reducing the range of spatial frequencies of the specturm of such type of pattern. On the contrary, at intermediate values of A we observed a transition to labyrinth-like patterns, followed by a transition back to spotted patterns as shown in Fig. 5.

9.2. Including a behavioural reduction of contacts at risk

We have seen that the strength A of the social distancing deeply impacts on patterns, even when $A < A_{cr}$. However, we verified that the overall size of the endemic prevalence remains close to I_e. Indeed, the above simulations, where $\phi(I) = 1$, were mainly aimed at showing the effect of the addition of pure spatial behavioural changes on the model (49)–(50). In the reality, spatial behavioural changes are in all cases paired with changes of behaviour that reduce the contacts at risks. This is modelled by means of a decreasing function $\phi(I)$ such that $\phi(0) = 1$. For this specific SIR model belonging to our family, we set as in [36,37,60–62]:

$$\phi(I) = \frac{1}{1 + q_h I^h}, \tag{52}$$

Note that defining $\theta_h = (q_h)^{-h}$ if $I = \theta_h$ it is $\phi(\theta_h) = 0.5$. In other word q_h measures the reactivity of the target population to the disease: the larger q_h is the higher is the behavioural reactivity to the spread of the infectious disease. The resulting

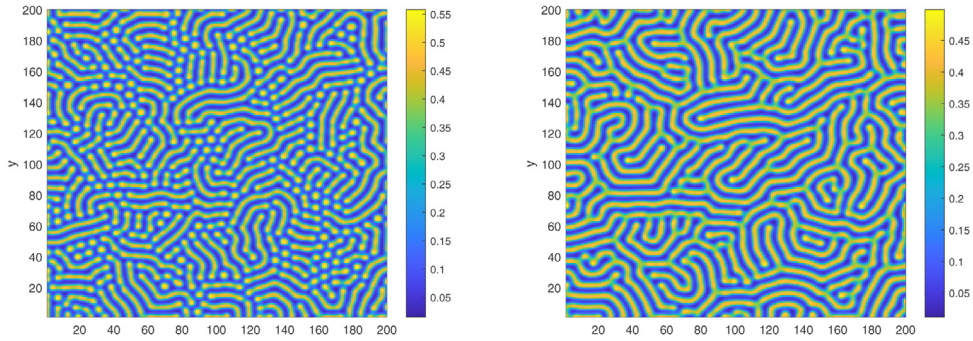

Fig. 5. Model (51)–(50). Role of the parameter A for $0 < A < A_{cr}$. Left panel: a mixed pattern with many residual spots and many 'labyrinth walls' of short length is observed at $A \approx 0.3A_c r$. Central panel: a labyrinth-like pattern is observed at $A \approx 0.5A_c r$ Right panel: a transition pattern were spots are re-emerging is observed at $A \approx 0.78A_c r$. Initial conditions and other parameters as specified in the text.

full model reads as follows:

$$\partial_t S = D_S \Delta S + div(\bar{A} S \nabla I) + \mu(1 - S) - \frac{\beta}{1 + q_h I^h} I^2 S \tag{53}$$

$$\partial_t I = D_I \Delta I + \frac{\beta}{1 + q_h I^h} I^2 S - (\mu + \nu) I \tag{54}$$

$$\partial_n I|_{\partial\Omega} = \partial_n S|_{\partial\Omega} = 0 \tag{55}$$

At $(\bar{A}, q_h) = (0, 0)$ one recovers the spatio-temporal model by Sun. In the spatially homogeneous setting ($D_S = \bar{A} = D_I = 0$). The case $h = 2$ is a particular case of the SIRS model proposed and investigated in [35–37] and extended in the spatio-temporal setting (i.e. $\bar{A} = 0$, $D_S \neq 0$, $D_I \neq 0$) by [29], whereas for $h = 1$ it is an example of the non–spatial ($D_S = \bar{A} = D_I = 0$) family of models proposed in [35].

9.2.1. Endemic equilibria and their spatio-temporal stability

Here we concisely illustrate some key features of the model for a generic value of h. At variance with [36,37,60–62], here we will focus as bifurcation parameter on q_h, which modulates the behavioural reactivity of the target population and as a consequence is biophysically the most specific parameter.

The analytical investigations are facilitated by setting

$$g(I) = \frac{\sigma}{\beta} \frac{1 + q_h I^h}{I}.$$

The homogeneous endemic equilibrium point solves the following system:

$$S = 1 - \sigma I \tag{56}$$

$$S = g(I) \tag{57}$$

yielding:

$$\beta I^2 - \frac{\beta}{\sigma} I + 1 = -q_h I^h.$$

It is easy to verify that for all $h > 0$ there are two endemic equilibria provided that

$$0 < q_h < q_h^*$$

and no endemic equilibria if $q_h > q_h^*$, where q_h^* is an increasing function of h. In other words: there is a minimal reaction threshold $\theta_h^* = (q_h^*)^{(-h)}$ such that if $\theta_h < \theta_h^*$ then the behavioural reaction suppress the possibility of endemic permanence of the disease in the population.

For $h \in \{1, 2, 3, 4\}$ q_h^* can be analytically computed. For example: $q_1^* = \beta/\sigma - 2\sqrt{\beta}$ and $q_2^* = 0.25\,(\beta/\sigma)^2 - \beta$. We denote the two endemic equilibria as follows: $E_1^{(h)}$ and $E_2^{(h)}$. They are such that (i) $I_{E_1^h} < I_{E_2^h}$; (ii) $\partial_h E_2^{(h)} < 0$ and $\partial_h E_1^{(h)} > 0$. For $\beta = 35.0$ and $\sigma = 2.8$, for example, one has that: $q_1^* \approx 0.6677$ and $q_2^* \approx 4.0625$.

At an equilibrium point the Jacobian matrix J of the non–spatial system reads as follows:

$$J_{11} = -\left(1 + \sigma \frac{I_e}{S_e}\right) < 0, \quad J_{12} = \sigma\left(-1 + \sigma \frac{I_e}{S_e} g'(I_e)\right)$$

$$J_{21} = \sigma \frac{I_e}{S_e}, \quad J_{22} = -\sigma \frac{I_e}{S_e} g'(I_e).$$

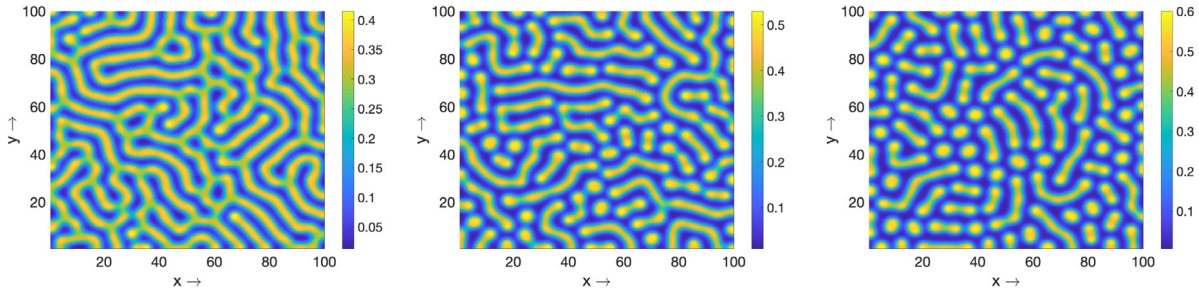

Fig. 6. Model (53)–(54). Spatial patterns exhibited by I for $A = 0$, $h = 2$, $q_2 = 2$. Left panel: $D_S = 5$; Central Panel: $D_S = 10$; Right Panel: $D_S = 15$.

the characteristic polynomial reads as follows

$$\lambda^2 + \left(1 + \sigma \frac{I_e}{S_e}\left(1 + g'(I_e)\right)\right)\lambda + \sigma \frac{I_e}{S_e}\left(\sigma + g'(I_e)\right) = 0.$$

Since, thanks to (56)–(57), it is $g'(I_{E_1^{(h)}}) < -\sigma$ then E_1^h is unstable. Concerning $E_1^{(h)}$, taking into the account that – again, thanks to (56)–(57) – $g'(I_{E_2^{(h)}}) > -\sigma$ holds it follows that if:

$$g'(I_e) > Max\left(-\sigma, -1 - \frac{S_e}{\sigma I_e}\right)$$

then $E_2^{(h)}$ is LAS.

Furthermore, if it is:

$$-\sigma < -1 - \frac{S_e}{\sigma I_e}$$

then even for

$$-\sigma < g'(I_e) < -1 - \frac{S_e}{\sigma I_e}$$

the equilibrium point is unstable.

Note that if for some value q_h^{**} of q_h is

$$1 + \sigma \frac{I_e}{S_e}\left(1 + g'(I_e)\right) = 0$$

then at $q_h = q_h^{**}$ a Hopf bifurcation occur and in the right neighbour of q_h^{**} a small harmonic periodic solution arises with pulsation

$$\omega_{Hopf} = \sqrt{\sigma \frac{I_e}{S_e}\left(\sigma + g'(I_e)\right)},$$

and period $T_{Hopf} = 2\pi/\omega_{Hopf}$.

For example, setting $\beta = 35$, $\sigma = 2.8$ and $h = 2$ and assuming $\eta = q_2$ then this yields that $E_2^{(2)}$ is LAS for $0 < q_2 < q_2^{**} \approx 2.34$, at $q_2 = q_2^{**}$ a Hopf bifurcation occur and for $q_2^{**} < q_2 < q_2^*$ the equilibrium point $E_2^{(2)}$ is unstable. In other words it exists a behavioural reaction threshold $\theta_h^{**} = 1/\sqrt{q_2}$ such that if $\theta_2^* < \theta_2 < \theta_2^{**}$ then $E_2^{(2)}$ is unstable.

As far as the onset of Turing bifurcations and of Turing–Hopf instability are concerned: (i) for $h = 1$, it follows that in absence of spatial distancing ($A = 0$) Turing bifurcations occur provided that D_S/D_I exceeds a threshold ρ^*. In such a case it also exists a strength of spatial behavioural reaction $A_{cr}^{(h=1)}$ such that the $E_2^{(1)}$ recovers its local stability; (ii) for $h \geq 2$, $g'(I_{E_2^{(2)}}) > 0$ then no Turing bifurcation occur since $D_I J_{11} + D_S J_{22}$ would be negative. Instead, if $g'(I_{E_2^{(2)}}) < 0$ then: (a) in absence of Hopf instability there onset of a Turing bifurcation for a sufficiently large D_S/D_I and its destruction for a sufficiently large A; (b) if additionally a Hopf instability is present (as illustrated above), then for a sufficiently large D_S/D_I a Turing–Hopf spatio-temporal instability occur and for sufficiently large A it is converted in a simple Hopf instability.

9.2.2. Turing patterning and its interplay with spatial behavioural response

Setting $\beta = 35$, $\sigma = 2.8$, $h = 2$, $q_2 = 2$, and $A = 0$, yielded that the Turing patterns occur for $D_S/D_I > r_{Turing}^{BeC} \approx 2.76$. This threshold is lower than the one observed in absence of behavioural impact on the contagion rate. Examples of spatial stationary patterns exhibited by the infectious are shown in Fig. 6 for three different values of D_S and $D_I = 1$.

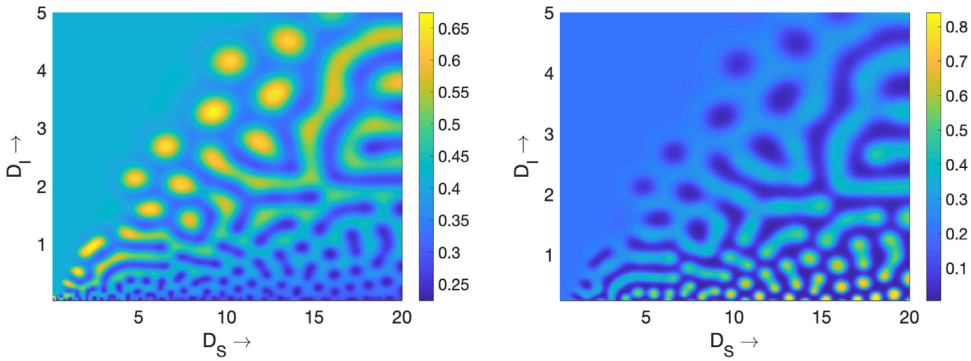

Fig. 7. Model (53)–(54). Visual summary of spatial patterns exhibited by S (panel(a)) and I (panel(b)) for a range of values of D_S and D_I.

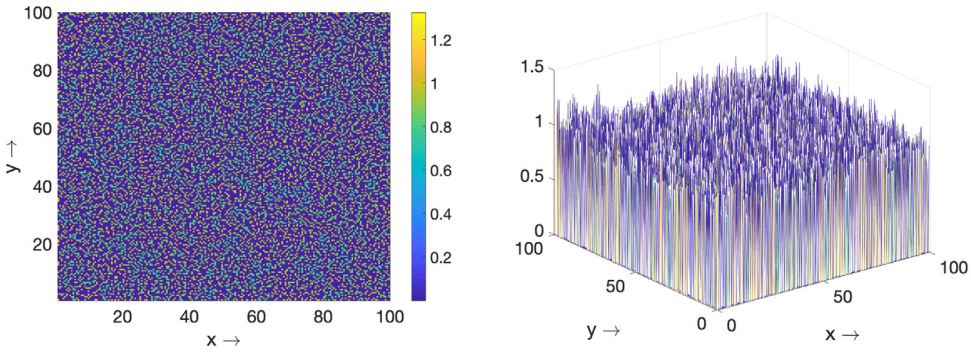

Fig. 8. Model (53)–(54). Heterogeneous distribution of susceptibles and infected individuals for $D_I = 0$. Other parameters: $h = 2$, $q_2 = 2$, $D_S = 10$.

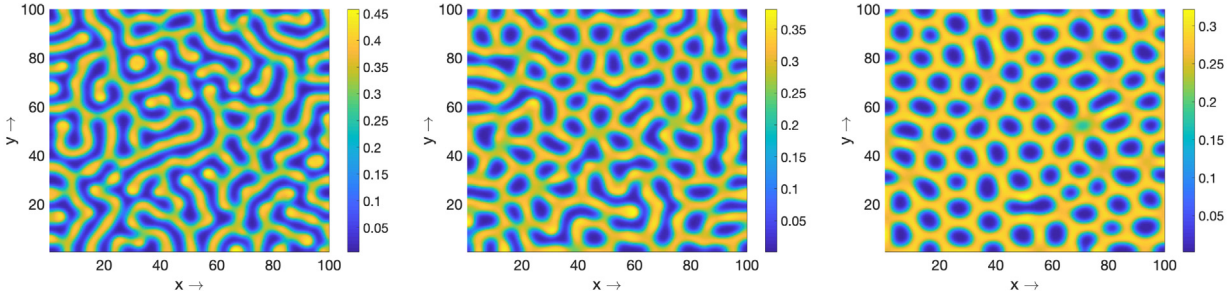

Fig. 9. Model (53)–(54). Impact of A: spatial patterns exhibited by I. Left Panel: $A = 0.3A_{cr}$; Central Panel: $A = 0.6A_{cr}$; Right Panel: $A = 0.9A_{cr}$.

A consolidated pattern diagram for susceptible and infected population for a range of values of D_S and D_I is presented in Fig. 7.

For $D_I = 0$ we find, as expected, an heterogeneous distribution of susceptibles and infected individuals with no particular pattern emerging. (see Fig. 8, where $D_S = 10$). The range of variation of population density is determined by the diffusivity of susceptibles.

Setting $D_S = 10$ and $D_I = 1$ yields that $A_{cr} \approx 9.57$, a value higher than the one of the case where behavioural dependence of the contagion rate was absent. Stationary patterns are presented in Fig. 9 for three values of $A \in (0, A_{cr})$. Also here, slowing down occurred. For example the left and central patterns presented in Fig. 9 are obtained at $t = 200$ whereas the stationary pattern presented in the right panel of Fig. 9 is at $t = 500$.

Fig. 10 shows a consolidated pattern diagram for a range of values of D_S and A.

Patterns shown in Fig. 9 are all visually dissimilar from the pattern at $A = 0$. An useful tool to compare the similarity of lattice-based maps is the bivariate moran index (BMI) [63]. We applied BMI to make a quantitative comparison of each pf the pattern shown in Fig. 9 and the pattern with $A = 0$. In all case there was no mutual spatial correlation between the maps $BMI \approx 0$.

The spatio-temporal pattern at $D_I = 0$ is very much sensitive with respect to the choice of D_S and we need to choose Δx and Δt judiciously in order to avoid numerical artefacts. An interesting phenomenon is observed for the parameter

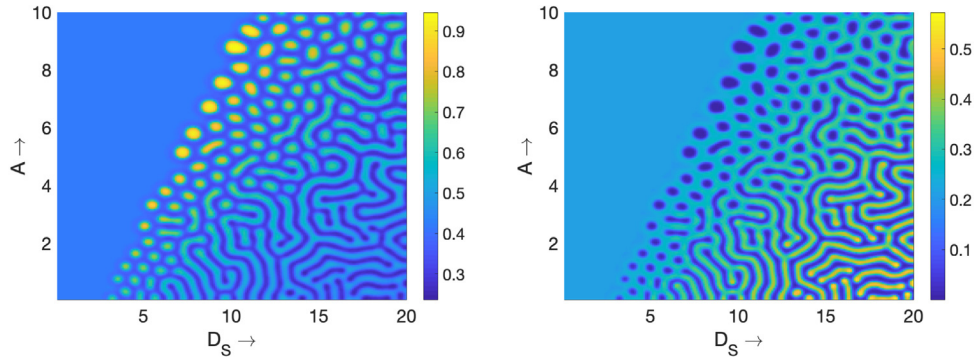

Fig. 10. Model (53)–(54). Visual summary of spatial patterns exhibited by S (panel(a)) and I (panel(b)) for a range of values of D_S and A.

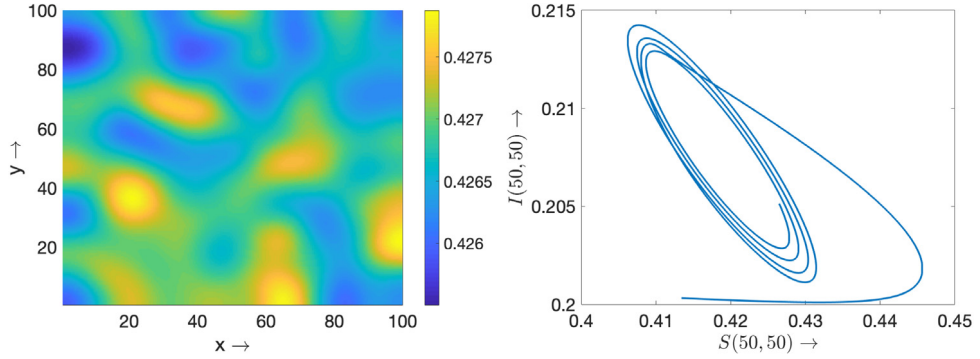

Fig. 11. Model (53)–(54). Spatio-temporal oscillations for $D_I = 0$, $D_S = 2$, $A = 7.66$. Left panel: $S(x, y, 1000)$; right panel: plot of $(mean(S)(t), mean(I)(t))$.

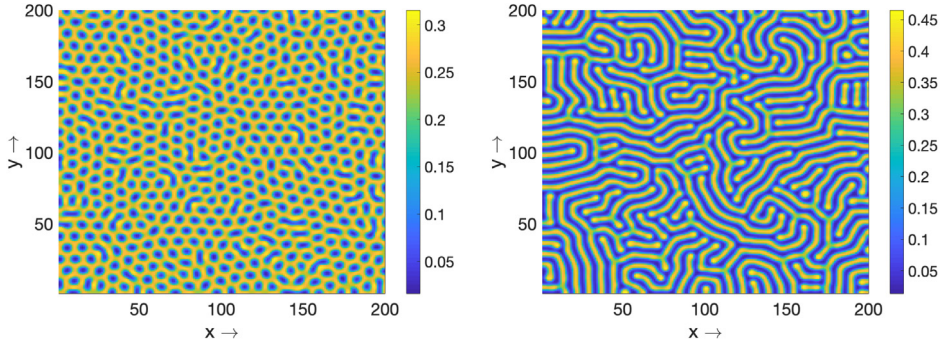

Fig. 12. Model (53)–(54). Turing–Hopf induced stationary spatial patterns of I for $A = 0$ and $D_S = 1$. Left panel: $D_S = 3$; Right panel: $D_S = 8$.

values $D_S = 2, A = 7.66$: spatio-temporally oscillating patterns with very mildly damped oscillations were observed with very small damping. Left panel of Fig. 11 show the spatial pattern of S at $t = 1000$, whereas its right panel shows the time evolution of spatial averages of S and I.

9.2.3. Turing–Hopf instability and its interplay with spatial behavioural response

Now we consider the spatio-temporal pattern formation for parameter values chosen from temporal Hopf domain, i.e. in the case $q_2 > q_2^{**} = 2.34$.

We first assumed $q_2 = 1.1q_2^{**}$, i.e. a value of q_2 close to the temporal Hopf bifurcation. For $A = 0$ and $D_I = 1$ we got that Turing–Hopf instability onsets for $D_S > 2.54$. Stationary spatial patterns for $D_S = 3$ and $D_S = 8$ are shown in Fig. 12.

In this case $A_{cr} = 9.57$ and spatial patterns for infected population are presented in Fig. 13 for three values of A.

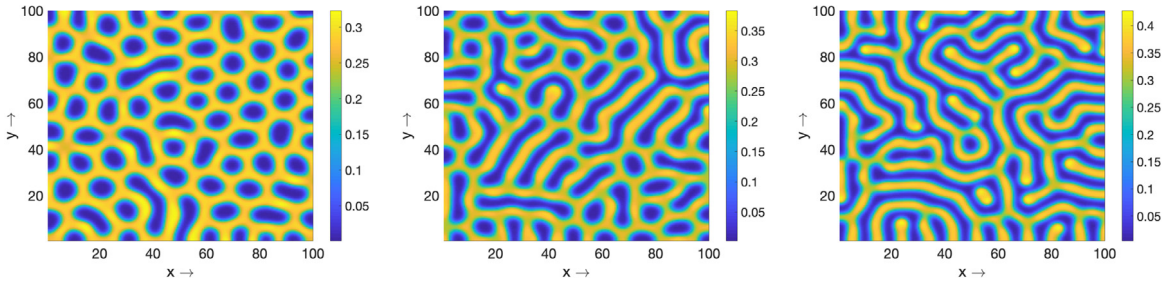

Fig. 13. Model (53)–(54). Turing–Hopf induced stationary spatial patterns for $q_2 = 1.1q_2^{**}$, $D_S = 10$, $D_I = 1$. Left panel: $A = 0.8A_{cr}$; Central panel: $A = 0.6A_{cr}$; Right Panel: $A = 0.3A_{cr}$.

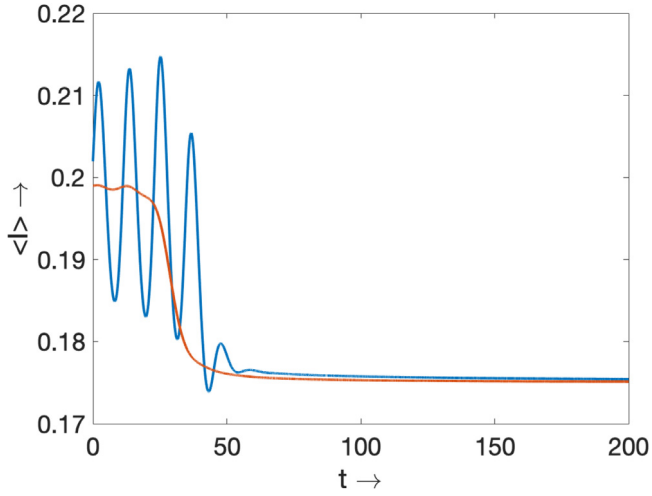

Fig. 14. Model (53)–(54). Plots of time evolution of spatial average of I starting with two different initial conditions and $q_h \approx 2.574$, $A = 0.8A_{cr}$. Blue curve is for the special IC and red curve is for random perturbation around homogeneous steady-state.

Additionally, we wanted to assess up to which extent the patterns are dependent on the initial conditions. Namely, we defined the following initial conditions:

$$S(x, y, 0) = S_{E_2}\,(1.01 + 0.01\cos(k_a y) + 0.01\cos(k_b x) + 0.01\gamma(x, y)) \tag{58}$$

$$I(x, y, 0) = I_{E_2}\,(1.01 + 0.01\cos(k_a x) + 0.01\cos(k_b y) + 0.01\eta(x, y)) \tag{59}$$

where

$$k_a = 0.01, k_b = 1$$

and $\eta(x, y)$ and $\gamma(x, y)$ at each point of the discretization mesh are random variables uniformly distributed in $(-1, 1)$. The spatial frequencies k_a and k_b were chosen as follows: k_b is such that $b_1(k_b) < 0$ and $\delta(k_b) < 0$, and k_b is close to the minimum of $b_0(k) < 0$.

We obtained stationary patterns that are different but qualitatively similar to those shown in Fig. 13.

However, for $A = 0.8A_{cr}$ the plot of $\langle I\rangle_{(x,y)}(t)$ shows (see Fig. 14) that if one adopts the initial conditions (58)–(59) or the above mentioned random perturbation of $E_2^{(2)}$ one gets close stationary values (and, as we have mentioned even the spatial pattern are qualitatively similar) but very different transients. Indeed, in the former case the transient is characterized by damped oscillations of relevant amplitude, in the latter case oscillations are small and far more damped. Note that the duration of the transient in both case is quite long w.r.t to the dynamics of the system since it is much larger than $1/\sigma$.

Finally, we further explored the domain $q_2 \in (q_2^{**}, q_2^{*})$ by setting $q_2 = 3.6$. In this case $A_{cr} = 15.053$ and spatial patterns for infected population are presented in upper panels of Fig. 15 for three values of A, including $A = 0$. Also here computing the BMIs evidenced a total lack of mutual spatial correlation between the patterns.

At variance with the case $q_2 = 1.1q_2^{**}$, here the patterns are strongly dependent on the initial conditions. For example, assuming the initial conditions (58)–(59) with $k_a = 0.05$, we obtained for $A = 0.8A_{cr}$ a very different stationary pattern (see lower panels of Fig. 15 and compare with its upper panels). Moreover, the plot of $\langle I\rangle_{(x,y)}(t)$ shows clearly that if one

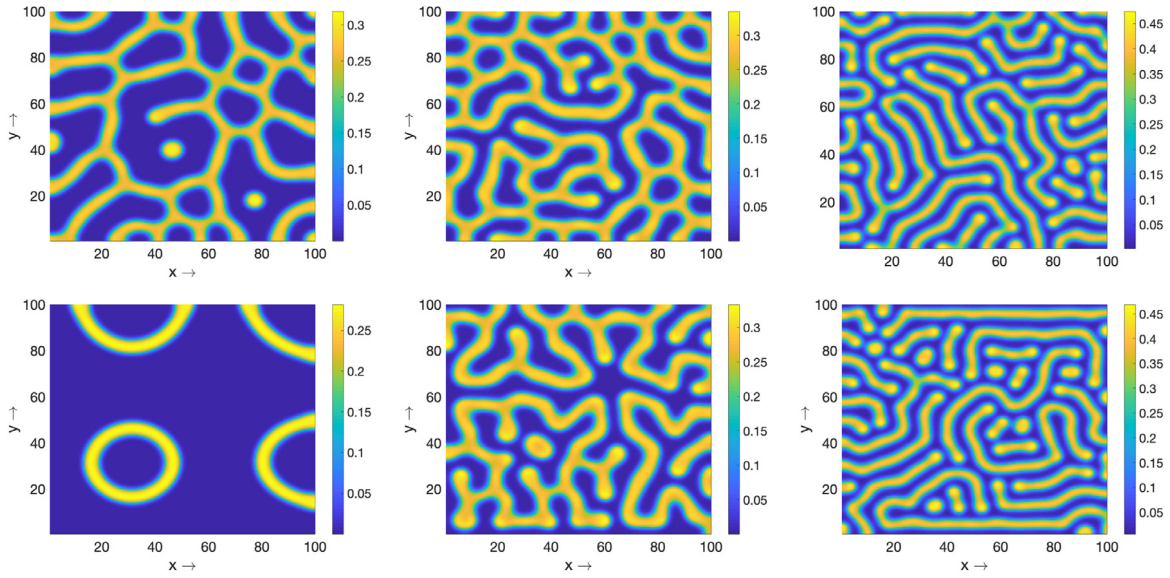

Fig. 15. Model (53)–(54). Turing–Hopf instability: impact of initial conditions and A onto stationary patterns. Upper panels: IC: random perturbations of E_2; Lower panels: special initial conditions with $k_a = 0.05$. Left panels: $A = 0.8A_{cr}$; Central panels: $A = 0.6A_{cr}$; Right Panels: $A = 0$.

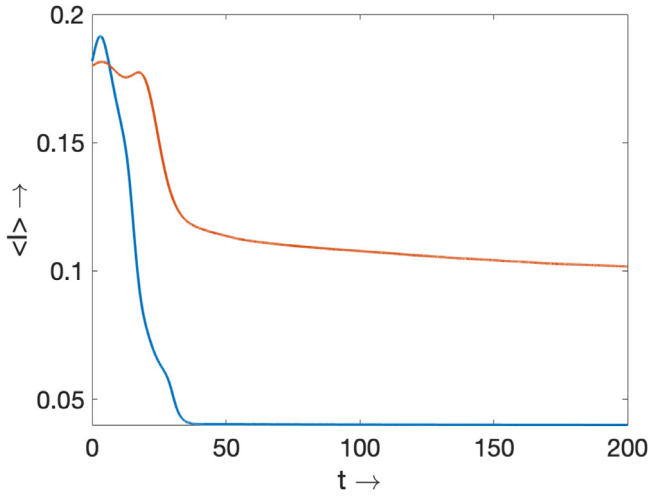

Fig. 16. Model (53)–(54). Plots of time evolution of spatial average of I starting with two different initial conditions and $A = 0.8A_{cr}$. Blue curve is for the special IC and red curve is for random perturbation around homogeneous steady-state.

adopts the initial conditions (58)–(59) the stationary average is much smaller than in the case of random initial conditions (see Fig. 16).

10. Concluding remarks

This work aimed to fill a gap in the current behavioural epidemiology literature by studying the effects of behavioural responses to epidemics threats within a reaction–diffusion setting. In particular, we investigated the combined impact of a localized "'social distancing'" response jointly with a spatial behavioural response, on the endemic pattern of a broad family of SIR and SIS infectious disease models. This was done by systematically benchmarking our results against two types of simpler models namely, (i) space homogeneous models including only a social distancing response by a prevalence-dependent contact rate, and (ii) spatially structured models with spatial movement and localized social distancing but not including a spatial behavioural response.

The analysis of the spatial model without spatial behavioural response provided a general relationship for the occurrence of Turing patterns, which can arise only when the diffusion of susceptible is faster than that of infectious

people. The analysis of the principal family of modela, also including the spatial behavioural response, provided conditions for the destruction of Turing pattern, which occurs in the presence of an adequately large strength A of spatial response ($A > A_{cr}$).

We also stressed that for $A \in (0, A_{cr})$ the increase of A induces transitions of the Turing pattern, due to the reduction of the interval of unstable frequencies. It is indeed well known that the content of the Fourier spectrum of a pattern influence its shape, see for example [64]. Reversing the viewpoint, a transition of patterns of an endemic disease (a phenomenon of paramount relevance, as stressed in [27]) could be due to changes in behaviour of the population.

In case of presence of Hopf–Turing spatio-temporal instability, we showed that if the 'force' of the spatial response is adequately large, then (due to the suppression of the Turing patterning) the system has a transition towards a pure Hopf instability, where the temporal symmetry breaking is prevalent. As it is well–known the Hopf–Turing instability is often associated to the onset of spatio-temporal chaos. This implies that the spatial behavioural response we have introduced here can have the effect of controlling spatio-temporal chaos.

In order to corroborate our theoretical inferences and to show possible nonlinear and transitory effects depending on A, we performed extensive numerical simulations on a behavioural SIR spatio-temporal model. To this aim we have initially considered the model proposed in [31] and investigated its bifurcation structure in dependence of the diffusion coefficients of S and I. Then we added the spatial behavioural component $\bar{A}div(S\nabla I)$ and finally a behavioural component of reduction of contagion. In all cases, our simulations not only confirmed our theoretical analysis but they allowed to go further. Namely, they showed that the theoretically predicted 'generic' impact of varying A under its threshold A_{cr} on pattern transitions produces in the specific analysed models a transition from labyrinth-like patterns to spotted patterns. Moreover, in the case of presence of Hopf–Turing spatio-temporal instability we showed that the impact of initial conditions although not leading to chaos in the example we considered (very likely due to the bistable nature of the model) is important: two close initial conditions can lead either to spatially similar but temporally dissimilar solutions, or to solutions that are both spatially and temporally dissimilar.

The main limitation of this work is that the spatial diffusion model under its classical hypotheses represents a crude approximation to real-world human mobility, which is qualitatively appropriate for nomadic populations only. More realistic modelling of human mobility behaviour are therefore needed to develop appropriate models of spatial responses to diseases threats pass to quantitative prediction , models that take into the account the inherent recurrent component of real spatial mobility – mainly daily commuting – of humans [8,9,65,66]. Another important point that we will investigate in the near future is related to the fact that the social–distancing phenomena we described here depends on the information individuals have of the spatial spread of the disease. Here we implicitly assumed that agents only use (or only dispose of) local information. However, information is most often of non-local nature and has its own dynamics [67]. The inclusion of the nonlocality of the information would lead to more sophisticated models of the flux J_S of susceptible subjects.

These two are the main challenge we will undertake in the future and it is questionable whether the reaction–diffusion partial differential equations settings might be the appropriate one to tackle this complexity so far preferably modelled by alternative paradigms such as large scale individual based models, metapopulation approaches [68,69] or network based modelling of the disease spread [11,42–44]. Importantly, both in network-based [45] and in metapopulation-based [46] epidemic models Turing patterning can occur in a network in a topology-dependent manner.

Nonetheless the concept of a spatial behavioural response remains a key one in behavioural epidemiology, and we feel that the present work represents a useful departure point.

Declaration of competing interest

The authors declare that they have no known competing financial interests or personal relationships that could have appeared to influence the work reported in this paper.

Acknowledgements

We would like to thank the two anonymous referees since their suggestions helped us to very significantly improve this work.

Appendix. Positiveness of $S(x, t)$

Here we mesoscopically derive the flux (2) and we show that the density $S(x, t)$ of susceptible subjects cannot become negative because of out behavioural assumption.

For the sake of the simplicity of notation, we will suppose to be in 1D. Let us consider a point x and an infinitesimal spatial interval $(x, x + h)$ and a temporal interval $(t, t + \delta)$. We have that

$$S(x, t + \delta) - S(t) = \delta\varphi_{epidemo} + \varphi^{in}_{Fickian} - \varphi^{out}_{Fickian} - \varphi^{out,R}_{behav} + \varphi^{in,R}_{behav} - \varphi^{out,L}_{behav} + \varphi^{in,L}_{behav}.$$

We have that $\delta\varphi_{epidemo}$ are the in and out fluxes due to the demography and to the contagion, the fluxes $\varphi^{in}_{Fickian} > 0$ and $-\varphi^{out}_{Fickian}$ are the Fickian input and output fluxes due to random walk and they are such that

$$\varphi^{in}_{Fickian} - \varphi^{out}_{Fickian} = h^2 D_S \partial^2_{xx} S + O(h^3).$$

All the above-listed fluxes are well-known. Let us now consider the in and out fluxes due to the spatial behavioural response. To start, $\varphi_{behav}^{out,R}$ is the flux of susceptible subjects that decide to move in $(x+h, x+2h)$ if and only if in $(x+h, x+2h)$ the density of infectious subjects is smaller. Thus

$$\varphi_{behav}^{out,R} = \bar{A}S(x,t)Max\left(I(x,t) - I(x+h,t), 0\right) \geq 0$$

Note that if $S(x,t) = 0$ then $\varphi_{behav}^{out,R}$.

Symmetrically, $\varphi_{behav}^{in,R}$ is the influx of susceptible subjects of $(x+h, x+2h)$ that move to $(x, x+h)$ if and only if the density of infectious subjects in $(x, x+h)$ is smaller. This yields

$$\varphi_{behav}^{in,R} = \bar{A}S(x+h,t)Max\left(I(x+h,t) - I(x,t), 0\right) \geq 0.$$

Similarly, we have:

$$\varphi_{behav}^{out,L} = \bar{A}S(x,t)Max\left(I(x,t) - I(x-h,t), 0\right) \geq 0$$

$$\varphi_{behav}^{in,L} = \bar{A}S(x-h,t)Max\left(I(x-h,t) - I(x,t), 0\right) \geq 0.$$

thus out microscopic model is well defined and such that it preserves the non–negativity of $S(x,t)$.

Developing $S(x+\pm h,t)$ and $I(x+\pm h,t)$ and neglecting the terms in $O(h^3)$, we get

$$\partial_t S\delta = \delta\varphi_{epidemo} + h^2\left(S_s\partial_{xx}^2 S + \bar{A}\partial_x S\partial_x I + \bar{A}S\partial_{xx}^2\right).$$

Proceeding to the limit $\delta \to 0$, $h \to 0$ under the usual diffusion restriction $(\delta/h^2) \to 1$ we get

$$\partial_t S + div(J_S) = \varphi_{epidemo}.$$

References

[1] V. Capasso, Mathematical Structures of Epidemic Systems, Springer, 1993.
[2] J.D. Murray, Mathematical Biology I: An Introduction, Springer, 2002.
[3] J.D. Murray, Mathematical Biology. II Spatial Models and Biomedical Applications, Springer, 2001.
[4] M. Martcheva, An Introduction to Mathematical Epidemiology, Springer, 2015.
[5] H. Malchow, S.V. Petrovskii, E. Venturino, Spatiotemporal Patterns in Ecology and Epidemiology: Theory, Models, and Simulation, Chapman and Hall/CRC, 2007.
[6] S. Anita, V. Capasso, Reaction-diffusion systems in epidemiology, 2017, arXiv preprint arXiv:1703.02760.
[7] M.L.C. Degli Atti, et al., Mitigation measures for pandemic influenza in Italy: an individual based model considering different scenarios, PLoS One 3 (3) (2008) e1790.
[8] M. Ajelli, et al., Comparing large-scale computational approaches to epidemic modeling: agent-based versus structured metapopulation models, BMC Infect. Dis. 10 (1) (2010) 190.
[9] M. Ajelli, P. Poletti, A. Melegaro, S. Merler, The role of different social contexts in shaping influenza transmission during the 2009 pandemic, Sci. Rep. 4 (2014) 7218.
[10] P. Manfredi, A. d'Onofrio, Modeling the Interplay Between Human Behavior and the Spread of Infectious Diseases, Springer, 2013.
[11] Z. Wang, et al., Statistical physics of vaccination, Phys. Rep. 664 (2016) 1–113.
[12] G. Chowell, H. Nishiura, Transmission dynamics and control of Ebola virus disease (EVD): a review, BMC Med. 12 (1) (2014) 196.
[13] G. Chowell, C. Viboud, L. Simonsen, S. Merler, A. Vespignani, Perspectives on model forecasts of the 2014–2015 Ebola epidemic in West Africa: lessons and the way forward, BMC Med. 15 (1) (2017) 42.
[14] J.R. Conrad, L. Xue, J. Dewar, J.M. Hyman, Modeling the impact of behavior change on the spread of Ebola, in: G. Chowell, J.M. Hyman (Eds.), Mathematical and Statistical Modeling for Emerging and Re-Emerging Infectious Diseases, Springer, 2016, pp. 5–23.
[15] D.P. Durham, E.A. Casman, S.M. Albert, Deriving behavior model parameters from survey data: self-protective behavior adoption during the 2009–2010 influenza a (H1N1) pandemic, Risk Anal.: An Int. J. 32 (12) (2012) 2020–2031.
[16] S. Towers, G. Chowell, Impact of weekday social contact patterns on the modeling of influenza transmission, and determination of the influenza latent period, J. Theoret. Biol. 312 (2012) 87–95.
[17] M. Springborn, G. Chowell, M. MacLachlan, E.P. Fenichel, Accounting for behavioral responses during a flu epidemic using home television viewing, BMC Infect. Dis. 15 (1) (2015) 21.
[18] G. Chowell, C. Ammon, N. Hengartner, J. Hyman, Transmission dynamics of the great influenza pandemic of 1918 in Geneva, Switzerland: Assessing the effects of hypothetical interventions, J. Theoret. Biol. 241 (2) (2006) 193–204.
[19] D. Rios-Doria, G. Chowell, Qualitative analysis of the level of cross-protection between epidemic waves of the 1918–1919 influenza pandemic, J. Theoret. Biol. 261 (4) (2009) 584–592.
[20] M.C. Bootsma, N.M. Ferguson, The effect of public health measures on the 1918 influenza pandemic in US cities, Proc. Natl. Acad. Sci. 104 (18) (2007) 7588–7593.
[21] D.B. Meade, F.A. Milner, An SIR model for epidemics with diffusion to avoid infection and overcrowding, in: Proceedings of the 13th IMACS World Congress on Computation and Applied Mathematics, vol. 3, 1991, pp. 1444–1445.
[22] F.A. Milner, R. Zhao, SIR model with directed spatial diffusion, Math. Popul. Stud. 15 (3) (2008) 160–181.
[23] M. Bendahmane, M. Langlais, A reaction-diffusion system with cross-diffusion modeling the spread of an epidemic disease, J. Evol. Equ. 10 (4) (2010) 883–904.
[24] S. Berres, R. Ruiz-Baier, A fully adaptive numerical approximation for a two-dimensional epidemic model with nonlinear cross-diffusion, Nonlinear Anal. RWA 12 (5) (2011) 2888–2903.
[25] S. Berres, R. Ruiz-Baier, Simulation of an epidemic model with nonlinear cross-diffusion, in: Numerical Methods for Hyperbolic Equations, CRC Press, 2012, p. 331.
[26] S. Berres, J. Gonzalez-Marin, On epidemic models with nonlinear cross-diffusion, in: 20th International Congress on Modelling and Simulation, Adelaide, Australia, 1–6 December 2013, vol. 3, 1991, pp. 317–323.

[27] G.-Q. Sun, M. Jusup, Z. Jin, Y. Wang, Z. Wang, Pattern transitions in spatial epidemics: Mechanisms and emergent properties, Phys. Life Rev. 19 (2016) 43–73.
[28] G. Sun, Z. Jin, Q.-X. Liu, L. Li, Pattern formation in a spatial S–I model with non-linear incidence rates, J. Stat. Mech. Theory Exp. 2007 (11) (2007) P11011.
[29] G.-Q. Sun, Z. Jin, Q.-X. Liu, L. Li, Chaos induced by breakup of waves in a spatial epidemic model with nonlinear incidence rate, J. Stat. Mech. Theory Exp. 2008 (08) (2008) P08011.
[30] M. Cui, T.-H. Ma, X.-E. Li, Spatial behavior of an epidemic model with migration, Nonlinear Dynam. 64 (4) (2011) 331–338.
[31] G.-Q. Sun, Pattern formation of an epidemic model with diffusion, Nonlinear Dynam. 69 (3) (2012) 1097–1104.
[32] T. Wang, Dynamics of an epidemic model with spatial diffusion, Physica A 409 (2014) 119–129.
[33] T. Wang, Pattern dynamics of an epidemic model with nonlinear incidence rate, Nonlinear Dynam. 77 (1–2) (2014) 31–40.
[34] V. Capasso, G. Serio, A generalization of the Kermack-McKendrick deterministic epidemic model, Math. Biosci. 42 (1–2) (1978) 43–61.
[35] H.W. Hethcote, P. Van den Driessche, Some epidemiological models with nonlinear incidence, J. Math. Biol. 29 (3) (1991) 271–287.
[36] S. Ruan, W. Wang, Dynamical behavior of an epidemic model with a nonlinear incidence rate, J. Differential Equations 188 (1) (2003) 135–163.
[37] Y. Tang, D. Huang, S. Ruan, W. Zhang, Coexistence of limit cycles and homoclinic loops in a SIRS model with a nonlinear incidence rate, SIAM J. Appl. Math. 69 (2) (2008) 621–639.
[38] A.M. Turing, The chemical basis of morphogenesis, Phil. Trans. R. Soc. Lond. B 237 (641) (1952) 37–72.
[39] B. Ermentrout, M. Lewis, Pattern formation in systems with one spatially distributed species, Bull. Math. Biol. 59 (3) (1997) 533–549.
[40] A. De Wit, G. Dewel, P. Borckmans, Chaotic Turing-Hopf mixed mode, Phys. Rev. E 48 (1993) R4191–R4194.
[41] B.T. Grenfell, A. Kleczkowski, S. Ellner, B. Bolker, Measles as a case study in nonlinear forecasting and chaos, Philos. Trans. R. Soc. Lond. Ser. A Math. Phys. Eng. Sci. 348 (1688) (1994) 515–530.
[42] L. Li, et al., Analysis of transmission dynamics for Zika virus on networks, Appl. Math. Comput. 347 (2019) 566–577.
[43] H.A.M. Malik, A.W. Mahesar, F. Abid, A. Waqas, M.R. Wahiddin, Two-mode network modeling and analysis of dengue epidemic behavior in Gombak, Malaysia, Appl. Math. Model. 43 (2017) 207–220.
[44] R. Pastor-Satorras, C. Castellano, P. Van Mieghem, A. Vespignani, Epidemic processes in complex networks, Rev. Modern Phys. 87 (3) (2015) 925.
[45] M. Duan, L. Chang, Z. Jin, Turing patterns of an SI epidemic model with cross-diffusion on complex networks, Physica A 533 (2019) 122023.
[46] P.S. Putra, H. Susanto, N. Nuraini, Turing patterns of non-linear SI model on random and real-structure networks with diarrhea data, Sci. Rep. 9 (1) (2019) 8892.
[47] C. Bauch, A. d'Onofrio, P. Manfredi, Behavioral epidemiology of infectious diseases: an overview, in: P. Manfredi, A. d'Onofrio (Eds.), Modeling the Interplay Between Human Behavior and the Spread of Infectious Diseases, Springer, 2013, pp. 1–19.
[48] J. Staiano, The impact of the plague on human behavior in seventeenth century europe, ESSAI 6 (1) (2008) 46.
[49] D. Steel, Plague writing: from Boccaccio to Camus, J. Eur. Stud. 11 (42) (1981) 88–110.
[50] H.-I. Kuo, C.-C. Chen, W.-C. Tseng, L.-F. Ju, B.-W. Huang, Assessing impacts of SARS and Avian Flu on international tourism demand to Asia, Tourism Manag. 29 (5) (2008) 917–928.
[51] E.P. Fenichel, N.V. Kuminoff, G. Chowell, Skip the trip: Air travelers' behavioral responses to pandemic influenza, PLoS One 8 (3) (2013) e58249.
[52] V. Capasso, A. Di Liddo, F. Notarnicola, L. Russo, Epidemic reaction-diffusion system with cross-diffusion: modeling and numerical solution, J. Biol. Systems 3 (03) (1995) 733–746.
[53] R.M. Colombo, E. Rossi, Hyperbolic predators vs. parabolic prey, Commun. Math. Sci. 13 (2) (2015) 369–400.
[54] R. Bürger, G. Chowell, E. Gavilán, P. Mulet, L.M. Villada, Numerical solution of a spatio-temporal predator-prey model with infected prey, Math. Biosci. Eng. 16 (1) (2018) 438–473.
[55] R. Bürger, G. Chowell, E. Gavilán, P. Mulet, L.M. Villada, Numerical solution of a spatio-temporal gender-structured model for hantavirus infection in rodents, Math. Biosci. Eng. 15 (1) (2018) 95–123.
[56] T. Hillen, K.J. Painter, A user's guide to PDE models for chemotaxis, J. Math. Biol. 58 (1) (2008) 183, https://doi.org/10.1007/s00285-008-0201-3.
[57] D.V. Efimov, A.L. Fradkov, Oscillatority of nonlinear systems with static feedback, SIAM J. Control Optim. 48 (2) (2009) 618–640.
[58] Y. Nishiura, Far-from-equilibrium Dynamics, American Mathematical Society, 2002.
[59] W.-M. Liu, H.W. Hethcote, S.A. Levin, Dynamical behavior of epidemiological models with nonlinear incidence rates, J. Math. Biol. 25 (4) (1987) 359–380.
[60] W.-m. Liu, S.A. Levin, Y. Iwasa, Influence of nonlinear incidence rates upon the behavior of SIRS epidemiological models, J. Math. Biol. 23 (2) (1986) 187–204.
[61] W. Wang, Epidemic models with nonlinear infection forces, Math. Biosci. Eng. 3 (1) (2006) 267.
[62] Z. Hu, et al., Bifurcations of an SIRS epidemic model with nonlinear incidence rate, Discrete Contin. Dyn. Syst. Ser. B 15 (3) (2011) 93–112.
[63] C. Robertson, C. Mazzetta, A. d'Onofrio, Regional variation and spatial correlation, in: P. Boyle, M. Smans (Eds.), Atlas of Cancer Mortality in the European Union and the European Economic Area 1993–1997, WHO Press, 2008, pp. 91–113.
[64] H. Shoji, Y. Iwasa, Labyrinthine versus straight-striped patterns generated by two-dimensional Turing systems, J. Theoret. Biol. 237 (1) (2005) 104–116.
[65] D. Balcan, A. Vespignani, Phase transitions in contagion processes mediated by recurrent mobility patterns, Nat. Phys. 7 (7) (2011) 581.
[66] C. Song, T. Koren, P. Wang, A.-L. Barabási, Modelling the scaling properties of human mobility, Nat. Phys. 6 (10) (2010) 818.
[67] X.-X. Zhan, et al., Coupling dynamics of epidemic spreading and information diffusion on complex networks, Appl. Math. Comput. 332 (2018) 437–448.
[68] M.J. Keeling, P. Rohani, Modeling Infectious Diseases in Humans and Animals, Princeton University Press, 2011.
[69] S. Meloni, et al., Modeling human mobility responses to the large-scale spreading of infectious diseases, Sci. Rep. 1 (2011) 62.